Biosensors and Bioelectronics 91 (2017) 687–691

Contents lists available at ScienceDirect

Biosensors and Bioelectronics

journal homepage: www.elsevier.com/locate/bios

Aptamer-molecularly imprinted sensor base on electrogenerated chemiluminescence energy transfer for detection of lincomycin

Shuhuai Li*, Chunhua Liu, Guihao Yin, Qun Zhang, Jinhui Luo*, Nanchun Wu

Analysis and Test Center of Chinese Academy of Tropical Agricultural Sciences, Haikou, 571101, China; Laboratory of Quality & Safety Risk Assessment for Tropical Products (Haikou) Ministry of Agriculture, Haikou, 571101, China

ARTICLE INFO

Keywords:
Dual recognition
Aptamer
Molecularly imprinted
lincomycin
Energy transfer

ABSTRACT

In this study, a biosensor with a dual recognition system comprising a molecularly imprinted polymer (MIP) and aptamers selective for lincomycin was fabricated. The MIP was synthesized by electropolymerization of carbon dots (C-dots)-tagged DNA aptamers combined with lincomycin and *o*-aminophenol on the gold-nanoparticle-functionalized graphene oxide (Au-GO)-modified electrode. Electrogenerated chemiluminescence (ECL) resonance energy transfer was observed between Au-GO and C-dots. After the C-dots accepted the energy, they acted as a signal indicator and exhibited enhanced signal intensity in the presence of target lincomycin. When lincomycin was competitively bound to DNA aptamers and MIP, it blocked the transfer of energy, and a decreased ECL signal was observed. Hence, a dual recognition method for the detection of lincomycin is realized. Using this strategy, the sensor exhibited a linear ECL response to lincomycin at concentrations from 5.0×10^{-12} mol/L to 1.0×10^{-9} mol/L. The detection limit of this assay was found to be 1.6×10^{-13} mol/L. This method was utilized to determine lincomycin residuals in meat samples with satisfactory results.

1. Introduction

Lincomycin (Rocco et al., 2012) is an antibiotic against bacteria, that is widely used in the feed and animal production industry. Some studies have suggested that the presence of lincomycin in animal-derived food may cause health problems (Sreeshitha et al., 2014). Hence, it is crucial to detect and monitor lincomycin residues in meat products as well as in the environment. Currently, high-performance liquid chromatography (HPLC) (Stypulkowska et al., 2015) or HPLC–mass spectrometry (HPLC–MS) (Dousa et al., 2006; Yi et al., 2015) are typically employed for the detection of lincomycin. However, both methods require the use of large-scale equipment and complex sample pretreatment. Hence, it is of significance to develop a sensitive, selective, cost-effective, and simple method for detecting lincomycin.

Molecularly imprinted polymers (MIPs) (Yu et al., 2002; Zamoragálvez et al., 2016) and aptamers (Kato et al., 2016; Wu et al., 2016) serving as recognition elements that can bind to specific target molecules, exhibit good performance in molecular recognition and separation. MIPs, which have been artificially synthesized, serve as a novel separation technique for precisely recognizing template molecules. Compared to traditional molecular-recognition-based separation techniques, MIPs exhibit the remarkable characteristic of excellent selectivity to substrates. Chao et al. (2016) have fabricated a fluorescence-based sensor combining the advantages of quantum dots (QDs) and MIPs on a glass substrate. After fabricating the sensor on both a 3-aminopropyltriethoxysilane (APS) and a 3-mercaptopropyltriethoxysilane (MPS)-modified glass substrate, APS exhibited significantly better performance than MPS as both the capping reagent of QDs and the functional monomer of tetracycline-templated MIPs. However, to meet the requirements of samples containing complex matrices, it is necessary to enhance the selective recognition of MIPs, attributed to the relatively limited recognition sites in the MIPs and their imprinted capacities (Rampey et al., 2004). With progress of research, aptamers have attracted immense interest; aptamers are single, short nucleic acid sequences (either DNA or RNA), which are typically selected by the systematic evolution of ligands by exponential enrichment (SELEX) (Darmostuk et al., 2015). On account of their remarkable characteristics, including high specificity, facile synthesis in vitro, and facile modification, as well as widely adopted target molecules, aptamers have been widely used for environmental monitoring (Reinemann et al., 2015) and medical examination (Abnous et al., 2017), particularly for the detection of pesticide residues and veterinary drugs (Bala et al., 2016; Lu et al., 2015). Our research group (Li et al., 2016) has reported an electrogenerated chemiluminescence sensing platform

* Corresponding authors.
E-mail addresses: happylishuhuai@163.com (S. Li), luocatas@21cn.com (J. Luo).

http://dx.doi.org/10.1016/j.bios.2017.01.038
Received 21 November 2016; Received in revised form 16 January 2017; Accepted 18 January 2017
Available online 19 January 2017
0956-5663/

based on carbon dot-tagged aptamers, serving as the recognition element, for the detection of carbofuran. The detection limit of this assay is reported to be 8.8×10^{-13} mol/L, which is better than that observed for traditional methods. Thus, the combination of MIPs with DNA aptamers as a recognition technology to achieve enhanced sensitivity and selectivity is worthy of investigation. Liu et al. (2016) have developed upconversion nanoparticles for the detection of enrofloxacin based on molecularly imprinting and biotinylated enrofloxacin aptamers. With the combined characteristics of the specific molecular recognition properties of MIPs and aptamers, the recognition ability of these nanoparticles is further enhanced. However, upconversion nanoparticles are unstable, and an improvement in sensitivity is necessary. Considering all factors, it is hypothesized that an electrogenerated chemiluminescence (ECL) sensor based on an aptamer–MIP is suitable for resolving these issues. ECL (Pan et al., 2015; Wang et al., 2015) is a type of luminescence produced during electrochemical reactions in solutions. It exhibits advantages of high sensitivity, a wide linear range, and a low detection limit, as well as controllability. With the transfer of energy from an electrochemical donor to ECL reagents, the signal intensity of ECL is significantly enhanced; this phenomenon is referred to as ECL resonance energy transfer (ECRET) (Guo et al., 2015; Yu et al., 2015). In particular, compared to conventional ECL sensors, ECRET exhibits potential for use in applications, attributed to the advantages of high sensitivity, wide dynamic concentration response range, and good stability. Thus, ECRET-based sensors have been widely utilized for analyzing pesticides (Cheng et al., 2014; Wu et al., 2012). However, an aptamer-MIP sensor based on ECRET has not been reported.

In this study, an aptamer-MIP sensor based on ECRET was fabricated on a gold-nanoparticle-functionalized graphene oxide (Au-GO) nanocomposite for signal amplification. As shown in Fig. 1, ECRET was observed between the Au-GO nanocomposite and C-dots; after accepting energy, the C-dots served as a signal indicator and exhibited enhanced signal intensity in the absence of lincomycin. Furthermore, the signal significantly improved because of the amplification effect from the Au-GO nanocomposite. When lincomycin was competitively bound to DNA aptamers and MIPs, it blocked the transfer of energy; hence, the ECL signal decreased. As a result, a new method for detecting lincomycin is established. Because of the dual recognition from the DNA aptamers and MIPs for the target molecule, this sensor exhibited increased selectivity for lincomycin compared to traditional sensors. Moreover, ECRET is an effective approach for improving the sensitivity. Therefore, the developed sensor exhibits high linearity, stability, and sensitivity, as well as good resolution for the detection of lincomycin.

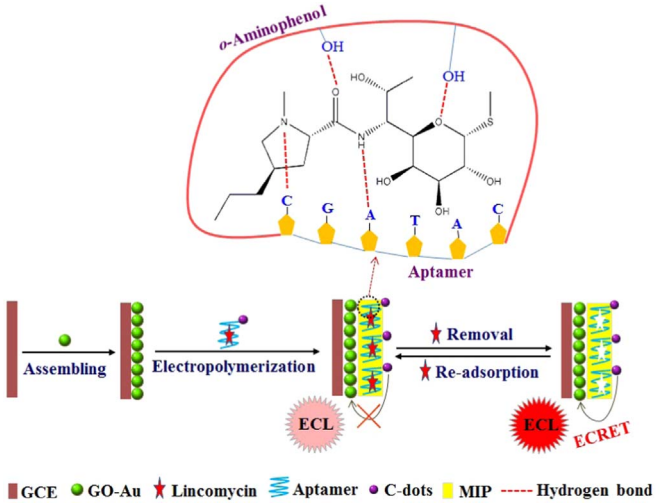

Fig. 1. Fabrication of the sensor for the detection of lincomycin.

2. Materials and methods

2.1. Chemicals, reagents, and electrochemistry

A lincomycin aptamer sequence (5'-C-dot-CGCGTGATGTGGTC-GATGCGATACGGTGAGT CGCGCCACGGCTACACACGTCTCAGCGA-3') and a random DNA sequence (5'-C-dot- GTCGATGCGCCACGCGCT-CATAGAGTGCTCAGCTCATGTCTCTCTGTCGACTCCACACGT-3') was synthesized using the SELEX kit obtained from Sangon Biotech Co. Ltd. (Shanghai, China). o-Aminophenol was purchased from J & K Scientific Ltd. (Beijing, China). Lincomycin and other pesticides were obtained from the Agricultural Environmental Quality Supervision and Testing Center of China. Graphite was obtained from Aladdin Reagent Co., Ltd. (Beijing, China). A 3×10^{-4} mol/L $K_3[Fe(CN)_6]/K_4[Fe(CN)_6]$ solution was prepared using 0.5 mol/L KCl. All aqueous solutions were prepared using ultrapure water (18.2 MΩ cm, Milli-Q, and Millipore).

ECL measurements were conducted on a Model MPI-E ECL analyzer (Xi'an Remex Instrument Co. Ltd., China) using a three-electrode system, which consisted of a Ag/AgCl electrode containing a saturated KCl solution, a platinum wire electrode, and a modified glassy carbon electrode (d = 3 mm) as the reference, auxiliary, and working electrodes, respectively. Electro-analytical measurements, such as cyclic voltammetry (CV) and alternating current (AC), were performed on a standard three-electrode workstation (CHI660E; Shanghai Chenhua Instrument Co. Ltd., Shanghai, China).

2.2. Preparation of the Au-GO modified electrode

GO was prepared from graphite by the Hummers method (Chen et al., 2013). First, 1.0 g of graphite was added 50 mL of vitriol, followed by the addition of 0.5 g KNO_3 and 5.0 g $KMnO_4$. Second, the mixture was placed in an ice-water bath and stirred for 4 h, then transferred to a water bath at 35 °C for 2 h. Third, 300 mL of ultrapure water was slowly added into the reaction mixture at 70 °C over 2 h. After the additional $KMnO_4$ was removed using 5% H_2O_2, the suspension was washed using 0.02 mol/L HCl and dried in a vacuum oven at 60 °C for 4 h, affording GO. GO (30 mg) and polyvinylpyrrolidone (0.06 g) were then dissolved in ultrapure water via ultrasonic dispersion. Next, 1.5 mL of $HAuCl_4$ was added, and stirred for 20 min. The mixture was heated to 180 °C using a high-temperature, high-pressure autoclave for 24 h. After cooling the mixture to room temperature, the solution was centrifuged, and the precipitate was washed several times with distilled water and ethanol. The final product was dried in vacuum under 50 °C for 10 h, affording the Au-GO nanocomposite. A glassy carbon electrodeelectrode (GCE) was dipped into acetone and ethanol and then ultrasonically cleaned for 5 min. Next, the obtained Au-GO nanocomposite was dispersed in ultrapure water (1 mg/mL), and 10 μL of the suspension was dropped on the GCE surface and dispersed. The electrode was subsequently gently washed with ultrapure water and allowed to dry naturally.

2.3. Fabrication of the aptamer-molecularly imprinted sensor

First, 1×10^{-4} mol/L of lincomycin was added to a 0.05 mol/L PBS solution (pH = 7.6) containing 1×10^{-6} mol/L of the aptamer to form the lincomycin–aptamer complex. Second, the MIP was prepared on the Au-GO-nanocomposite-film-modified GCE by electropolymerization. *o*-Aminophenol (0.01 g) was dissolved in 6 mL of 0.05 mol/L Tris-HCl buffer (pH = 8.0), and 4 mL of the lincomycin–aptamer complex prepared above was added and mixed for 2 min. CV was performed over a potential range of 0 – 1.2 V for 20 cycles. After washing to remove the lincomycin templates, the aptamer-molecularly imprinted sensor was obtained with the imprinting cavities. Non-molecularly imprinted polymer (NIP) was fabricated by the same method, but without the lincomycin template. A random DNA sequence was used instead of the aptamer to prepare the aptamer-

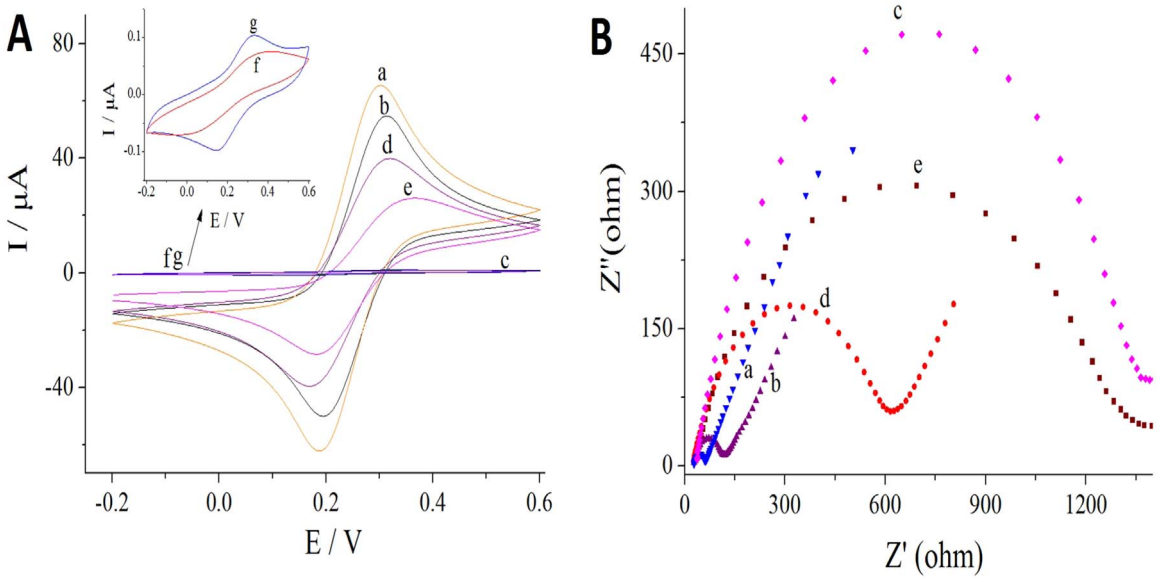

Fig. 2. (A) CV of the MIP and NIP sensors under different conditions: a. bare GCE; b. GO-Au modified GCE; c. MIP-modified GCE; d. MIP-modified GCE after the removal of lincomycin; e. MIP-modified GCE after the rebinding of lincomycin; f. NIP-modified GCE electrode; g. NIP-modified GCE after washing. (B) AC measurement of MIP films: a. bare GCE; b. GO-Au modified GCE; c. MIP-modified GCE; d. MIP-modified GCE after the removal of lincomycin; e. MIP-modified GCE after rebinding of lincomycin.

molecularly imprinted sensor in the contrast test.

2.4. Electrochemical and ECL measurements

Electrochemical experiments were performed in a 2×10^{-4} mol/L $K_3[Fe(CN)_6]/K_4[Fe(CN)_6]$ solution containing 0.02 mol/L of KCl. CV measurements were performed over a potential range from 0.2 to 0.6 V at a scan rate of 50 mV/s. AC measurements were performed at a potential of 0.19 V over a frequency range of 100 mHz – 100 kHz with an alternating voltage of 5 mV. ECL measurements were conducted in 10 mL of 0.01 mol/L Tris-HCl buffer (pH 8.0). CV measurements were conducted from −0.2 V to 0.8 V at a scan rate of 100 mV/s. The voltage of the photomultiplier tube was set to 800 V. The ECL signal-time curve was obtained by continuous potential scanning for five cycles at a magnification of 4. ECL signals were recorded for various lincomycin concentrations.

2.5. Sample treatment

Meat samples (5.00 g) were added to 20 mL of acetonitrile and ultrasonicated for 20 min, then transferred into a 50 mL flask for evaporation and drying on a rotary evaporator. The final residue was dissolved in 1.0 mL of methanol.

3. Results and discussion

3.1. Evaluation of the Au-GO nanocomposite

Transmission electron microscopy (TEM), ultraviolet–visible (UV-Vis) absorption spectroscopy, Fourier transform infrared spectroscopy (FTIR), and X-ray photoelectron spectroscopy (XPS) were employed to characterize the Au-GO nanocomposite. As shown in Fig. S1A, GO was observed as a thin, transparent slice, with a smooth, flat surface. The edge of the slice was wrinkled, indicating that GO comprises few layers. Spherical Au nanoparticles with an average diameter of 8 nm were scattered on the GO surface. Fig. S1B shows the UV–Vis spectrum of the GO-Au composite. Strong absorption was observed near 240 nm for GO and Au-GO (curves a and b, respectively), attributed to the π–π* transition of C–C in GO. On the other hand, additional absorption was observed near 520 nm (curve b) for Au-GO, attributed to the surface plasma resonance absorption peak of Au nanoparticles. From the XPS spectrum shown in Fig. S1C, intense signals were observed at 285.5 eV, 401.0 eV, and 532.5 eV, corresponding to C 1 s, N 1 s, and O 1 s, respectively. In particular, Au 4 f was observed at 84.0 eV and 87.7 eV. From the XRD pattern of the Au-GO composite in Fig. S1D, clear well-defined peaks corresponding to highly crystalline nanoparticles were observed. The XRD reflection at 11.5 was attributed to GO (curve a) (Yang et al., 2009). On the other hand, in Au-GO (curve b), the characteristic reflection for GO at 10.8 was not observed. Four major reflections were observed at 38.1, 43.4, 64.8, and 77.6, attributed to the (111), (200), (220), and (311) crystal planes of Au (Aromal et al., 2012), respectively. The results indicated that Au-GO was successfully prepared.

3.2. Polymerization of the MIP

The electropolymerization of *o*-aminophenol and the lincomycin–aptamer complex in Tris-HCl buffer (pH = 8.0) was investigated by CV over the potential range of 0 to +1.2 V. As shown in Fig. S2, a distinct, irreversible oxidation peak was observed for *o*-aminophenol at 0.78 V. With increasing number of cycles, the oxidation peak current for *o*-aminophenol continuously decreased because of the formation of the compact nonconducting polymer film, which covered the Au-GO-modified GCE surface. Nevertheless, by increasing the number of cycles to 20, the current density of the oxidation peak became smaller, indicating that the MIP film had formed on the electrode surface.

3.3. Evaluation of the MIP

Because of the absence of lincomycin redox peaks in the potential range from −0.2 to +0.8 V, $K_3[Fe(CN)_6]/K_4[Fe(CN)_6]$ was used as a redox probe to investigate the formation of the MIP film on the GCE electrode via CV and AC measurements. As shown in Fig. 2A, the current response for Au-GO/GCE (curve b) was significantly reduced compared with that for GCE (curve a), attributed to the fact that Au-GO prevented the redox probe from reaching the GCE surface. With the assembly of *o*-aminophenol and the lincomycin–aptamer complex on the modified electrode, the blockade was further strengthened, resulting in the continued decrease of the current response (curve c). However, after the removal of lincomycin from the MIP, the blockade receded, and the current response increased again (curve d). When lincomycin from the sample was re-adsorbed onto the MIP, the

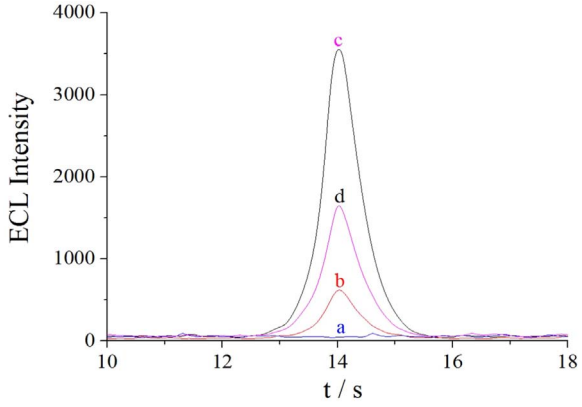

Fig. 3. ECL of the sensor under different conditions: a. ECL of GO-Au; b. ECL of C-dots; c. ECL of C-dots in the presence of GO-Au; d. ECL of C-dots of the sensor after the adsorption of lincomycin in the presence of GO-Au.

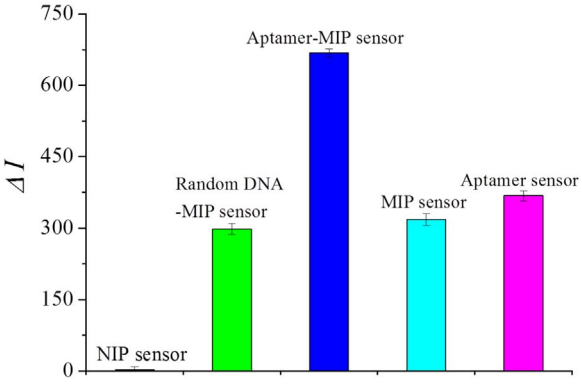

Fig. 4. Dual recognition ability for the aptamer–MIP sensor.

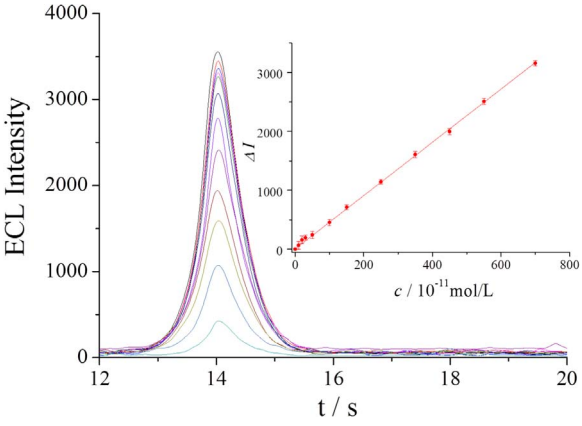

Fig. 5. Current response of the sensor with re-adsorbed lincomycin at different concentrations. a–i: (0, 5, 15, 30, 60, 100, 200, 350, 500, 600, 800, 1000) × 10^{-12} mol/L lincomycin. Potential range was −0.3 to 0.8 V.

blockade was strengthened again, and the current response decreased (curve e). The inset map in Fig. 2A shows the CVs of the NIP. With the formation of the NIP film on the electrode surface, the current response decreased (curve f). After elution, the peak current was nearly unchanged (curve g). Hence, the template molecule doped in the MIP film and non-cavities did not serve as channels for the transport of electrons. Meanwhile, the resistance of the modified electrode gradually increased with the modification of the GCE surface with Au-GO and MIP (Fig. 2B, curves a–c). The resistance of the modified electrode decreased with the removal of lincomycin from the MIP (Fig. 2B, curve d), but it increased again with the re-adsorption of lincomycin onto the MIP (Fig. 2B, curve e).

3.4. Investigation of the ECRET system

The ECRET system between Au-GO and C-dots on the DNA aptamer was investigated. As shown in Fig. 3, an ECL response was not observed for Au-GO (curve a). However, a clear ECL signal was observed for C-dots at a specific voltage (curve b), attributed to the stimulation of the C-dots. The ECL signal for C-dots was clearly enhanced by Au-GO (curve c). The ECRET mechanism possibly involves the activation of Au-GO to the excited state, thereby making it an efficient electron donor. C-dots accept energy from Au-GO, which improves the efficiency of excitation and results in high photostability and strong ECL. With the re-adsorption of lincomycin onto the MIP, the ECL intensity for C-dots obviously decreased (curve d), attributed to the binding of aptamers to lincomycin and the subsequent structural change; these effects attenuated the transfer of energy from GO-Au to C-dots; hence, effective ECRET occurred between GO-Au and C-dots.

3.5. Dual recognition of the aptamer–MIP sensor

The identification ability of the aptamer–MIP sensor was compared with those of the aptamer sensor, MIP sensor, NIP sensor, and aptamer–NIP sensor. The ECL intensity was measured before and after the re-adsorption of 2.0 × 10^{-10} mol/L lincomycin onto each of the above-mentioned sensors. As shown in Fig. 4, the ECL intensity for the NIP sensor exhibited almost no change, caused by the absence of specific recognition sites for lincomycin. Hence, lincomycin is not re-adsorbed onto the sensor. On the contrary, the ECL intensity for the aptamer and MIP sensors significantly decreased because both these sensors contain specific recognition sites for lincomycin. Meanwhile, the ECL intensity for the aptamer–NIP sensor, in which aptamers were randomly polymerized within the polymer layer, did not significantly change, indicating that the specific aptamer recognition sites are covered. However, the aptamer–MIP sensor exhibited a more significant reduction of ECL intensity compared with those observed for the other sensors, indicative of the dual recognition ability. Further tests showed that the ECL intensity for the random DNA–MIP sensor significantly decreased like that for the MIP sensors, because the recognition sites relied mostly on MIP. This indicated that lincomycin was not recognized by the random DNA.

Table 1
Results of sample assay and recoveries.

Samples	This method 10^{-11} mol/L (n=5)	RSD %	HPLC-MS method 10^{-11} mol/L (n=5)	Added 10^{-11} mol/L	Total found 10^{-11} mol/L (n=5)	RSD %	Recoveries %
Chicken	7.82	3.25	7.79	5.00	12.68	4.33	97.2
Duck	Not detected	–	Not detected	5.00	4.51	3.98	90.2
Crucian	Not detected	–	Not detected	10.00	10.05	4.08	100.1
Pork	Not detected	–	Not detected	10.00	89.90	2.58	89.9
Crab	6.22	2.84	6.31	20.00	26.85	3.24	103.1
Beef	Not detected		Not detected	20.00	18.90	3.36	94.5
Mutton	Not detected	–	Not detected	25.00	26.12	3.18	104.5

3.6. Optimization of experimental conditions

Experimental conditions, i.e., times for template removal and re-adsorption, buffer solution, and pH, were optimized for the detection of lincomycin. The removal of the lincomycin template was performed in formic10 mL 0.01 mol/L NaOH solution. The current intensity was measured every 2 min (Fig. S3); the current intensity gradually increased and then remained constant after 8 min. Thus, the optimum time for the removal of lincomycin was 8 min (curve a). The re-adsorption of the template was performed using 2.0 $\times 10^{-10}$ mol/L lincomycin. As more and more lincomycin was re-adsorbed, the inhibitory effect for ECRET was enhanced, and the current intensity gradually decreased. The minimum current intensity was obtained after 10 min. Thus, the optimum time for the re-adsorption of lincomycin was 8 min, which was utilized in the following assays (curve b). Effects of different buffers and pH were also evaluated. Three buffer solutions—0.01 mol/L of a borax buffer solution, 0.01 mol/L of a Tris-HCl buffer solution and 0.01 mol/L of a PBS solution (pH 8.0)—were investigated. The maximum current intensity was observed for the Tris-HCl buffer solution. The effect of pH using the Tris-HCl buffer solution was also investigated using the sensor for the re-adsorption of 2.0 × 10^{-10} mol/L lincomycin, and Fig. S4 shows the results. The current intensity increased with pH until it reached a maximum at pH 8.0; hence, pH 8.0 was selected as the optimum pH.

3.7. Calibration curve

The developed sensor was applied to the quantitative determination of lincomycin. Fig. 5 shows the ECL responses of the proposed aptamer–MIP sensor to different concentrations of lincomycin. From the experimental results, the relationship between the lincomycin concentration c and the increase in the current intensity ΔI was in the range from 5.0 × 10^{-12} to 1.0 × 10^{-9} mol/L. The linear regression fit was $\Delta I = 3.09\ c\ (10^{-12}\ \text{mol/L}) + 50.1$, with a correlation coefficient r of 0.999. The detection limit (*DL*) was 1.6 × 10^{-13} mol/L ($DL = KSb / a$, $K = 3$). Compared with previously published studies, the MIP sensor with a dual catalytic effect is more sensitive and has a low detection limit (Table S1).

3.8. Selectivity of the sensor

The selectivity of the aptamer–MIP sensor for lincomycin was analyzed using several common veterinary drugs, including tetracycline, clindamycin, illotycin, chloromycetin, enrofloxacin, ciprofloxacin, oxytetracycline, streptomycin, ephedrine, and vibramycin, with either similar or different chemical structures. Detection was performed as described above using 2.0 × 10^{-8} mol/L of each commercial veterinary drug in 1.0 × 10^{-10} mol/L lincomycin. As shown in Fig. S5, the ECL tests exhibited only minor changes (relative deviation < 5.0%) with or without addition of the above-mentioned drugs. Thus, drugs with structures similar to that of lincomycin are not identified by the aptamer, strongly suggesting that the aptamer sensor exhibits good selectivity for lincomycin.

3.9. Reproducibility and stability of the sensor

The reproducibility and stability of the sensor were studied. A relative standard deviation (RSD) of 3.4% was obtained by measurement of the ECL intensities for five different sensors, which indicated good sensor-to-sensor reproducibility. Additionally, an RSD of 4.5% was obtained by measurement of the ECL intensities using the same sensor in five measurements. The sensors were stored in the shade when not in use. The ECL response detected every two days was nearly unchanged. This indicated that the sensor exhibited good reproducibility and stability.

3.10. Detection of lincomycin in real samples

The proposed method was applied to the detection of lincomycin in actual meat samples. Sample pretreatment was performed as outlined in Section 2.5. The detection results from our sensor were compared with the results obtained from HPLC–MS analysis using the same samples. As shown in Table 1, recoveries between 89.9% and 104.5% were observed. The detection results with our sensor were consistent with those obtained from HPLC-MS. These analyses indicated that the developed sensor can be used to analyze the amount of lincomycin in actual samples.

4. Conclusions

In summary, this work combined an MIP and aptamer to introduce an aptamer-MIP sensor. The sensor showed high sensitivity and selectivity for lincomycin detection due to dual recognition, and is a potential new strategy for pesticide and veterinary drug detection. However, the stability of the DNA aptamer and the imprinted capacity in the sensor need further improvement; these will be the key problems to solve in future studies.

Acknowledgements

The authors gratefully acknowledge the financial support received from the Fundamental Scientific Research Funds of the Chinese Academy of Tropical Agricultural Sciences (No. 1630042015011 and 1630042015009).

Appendix A. Supporting information

Supplementary data associated with this article can be found in the online version at doi:10.1016/j.bios.2017.01.038.

References

Abnous, K., Danesh, N.M., Alibolandi, M., Ramezani, M., Taghdisi, S.M., Emrani, A.S., 2017. Sens. Actuators: B. Chem. 240, 100–106.
Aromal, S.A., Babu, K.V.D., Philip, D., 2012. Spectrochim. Acta A 96, 1025–1030.
Bala, R., Kumar, M., Bansal, K., Sharma, R.K., Wangoo, N., 2016. Biosens. Bioelectron. 85, 445–449.
Chao, M.R., Hu, C.W., Chen, J.L., 2016. Anal. Chim. Acta 925, 61–69.
Chen, J., Yao, B., Li, C., Shi, G., 2013. Carbon 64, 225–229.
Cheng, Y., Lei, J., Chen, Y., Ju, H., 2014. Biosens. Bioelectron. 51, 431–436.
Darmostuk, M., Rimpelova, S., Gbelcova, H., Ruml, T., 2015. Biotechnol. Adv. 33, 1141–1161.
Dousa, M., Sikac, Z., Halama, M., Lemr, K., 2006. J Pharm. Biomed. Anal. 40, 981–986.
Guo, Z., Kong, H., Yang, F., Chen, T., 2015. Sens. Actuators: B. Chem. 220, 270–278.
Kato, T., Shimada, I., Kimura, R., Hyuga, M., 2016. Chem. Commun. 52, 4041–4044.
Li, S., Wu, X., Liu, C., Yin, G., Luo, J., Zhi, X., 2016. Anal. Chim. Acta 941, 94–100.
Liu, X., Ren, J., Su, L., Gao, X., Tang, Y., Ma, T., Zhu, L., Li, J., 2016. Biosens. Bioelectron. 87, 203–208.
Lu, C., Tang, Z., Liu, C., Kang, L., Sun, F., 2015. Anal. Bioanal. Chem. 407, 5859–5859.
Pan, H., Shen, Y., Luan, L., Lu, K., Duan, J., Hu, B., 2015. J Phys. Chem. C 119, 8089–8094.
Rampey, A.M., Ii, R.J.U., Rushton, G.T., Iseman, J.C., R.N.S., Shimizu, K.D., 2004. Anal. Chem. 76, 1123–1133.
Reinemann, C., Fritsch, U.F.V., Rudolph, S., Strehlitz, B., 2015. Biosens. Bioelectron. 77, 1039–1047.
Rocco, L., Peluso, C., Stingo, V., 2012. Environ. Toxicol. 27, 598–604.
Sreeshitha, G.S., Venkatachalam, D., Dumka, V.K., 2014. Trop. Anim. Health Pro. 46, 1099–1102.
Stypulkowska, K., Blazewicz, A., Brudzikowska, A., Grzeskiewicz, M.W., Sarna, K., Fijalek, Z., 2015. J Pharm. Biomed. Anal. 112, 8–14.
Wang, Z., Yan, Z., Sun, N., Liu, Y., 2015. Biosens. Bioelectron. 68, 771–776.
Wu, D., Katilius, E., Olivas, E., Dumont, M.M., Walt, D.R., 2016. Anal. Chem. 2016 (88), 8385–8389.
Wu, M.S., Shi, H.W., He, L.J., Xu, J.J., Chen, H.Y., 2012. Anal. Chem. 84, 4207–4213.
Yang, D., Velamakanni, A., Bozoklu, G., Park, S., Stoller, M., Piner, R.D., Stankovich, S., Jung, I., Field, D.A., Ventrice, C.A., 2009. Carbon 47, 145–152.
Yi, X., Bayen, S., Kelly, B.C., Li, X., Zhou, Z., 2015. Anal. Bioanal. Chem. 407, 1–13.
Yu, Y., Lu, C., Zhang, M., 2015. Anal. Chem. 87, 8026–8032.
Yu, Y., Ye, L., Haupt, K., Mosbach, K., 2002. Angew. Chem. Int. Edit. 41, 4459–4463.
Zamoragálvez, A., Aitlahcen, A., Mercante, L.A., Moralesnarváez, E., Amine, A., Merkoçi, A., 2016. Anal. Chem. 88, 3578–3584.